*Sensors and Materials*, Vol. 34, No. 7 (2022) 2771–2790
MYU Tokyo



S & M 3005

# Hybrid Charging and Storage Design in Sustainable Solar-powered Wireless Sensor Node

Lu Wang,[1,2†] Dongsheng Li,[1,2†] Yintao Ma,[1,2] Libo Zhao,[1,2*]
Yao Chen,[1,2] Junlong Zhang,[1,2] Zhuangde Jiang,[1,2] and Ryutaro Maeda[1,2**]

[1]State Key Laboratory for Manufacturing Systems Engineering,
International Joint Laboratory for Micro/Nano Manufacturing and Measurement Technologies,
Collaborative Innovation Center of Suzhou Nano Science and Technology,
Xi'an Jiaotong University, Xi'an 710049, China
[2]School of Mechanical Engineering, Xi'an Jiaotong University, Xi'an 710049, China

(Received November 26, 2021; accepted February 9, 2022)

***Keywords:*** solar energy harvesting, wireless sensor node, power management, illumination monitoring, lithium battery charging

In view of the large scale and distributed characteristics of transformers, which lead to inconvenient manual inspection and state monitoring, and the limited energy of batteries restricting the development of wireless sensor nodes (WSNs), WSNs powered by solar energy are a promising approach. We propose a power management circuit for dual energy storage and dual-channel charging of a supercapacitor and a lithium battery with four modes to deal with the different charging currents of photovoltaic power generation under strong and weak light illumination, as well as the time mismatch between the energy harvesting power and WSN consumption power. We designed a low-power WSN with temperature, humidity, vibration, and illumination sensors in a low-duty-cycle operation mode with an average current consumption of 4.96 mA. Our solar power management circuit with undervoltage lockout (UVLO), maximum power point tracking (MPPT), quick charging, and a sustainable output characteristic is designed by LTspice simulation and verified by experiment in alternating light outdoors. The experiment demonstrates sustainable autonomous wireless sensing by dual charging and the feasibility of our storage design for solar energy harvesting, indicating its potential application in grid transformers.

## 1. Introduction

Monitoring the condition of transformers in a grid is valuable for improving the reliability and economy of the power supply system.(1) With the rise of the industrial Internet of Things (IoT), various applications based on the IoT have improved our lives, such as smartphones, smart speakers, home safety systems, and wearable electronic products.(2) Also, time- and labor-consuming manual inspections and troubleshooting methods are gradually being replaced by monitoring using wireless sensor nodes (WSNs).(3) At present, most industrial monitoring WSNs

*Corresponding author: e-mail: libozhao@mail.xjtu.edu.cn
**Corresponding author: e-mail: darwin.sea@gmail.com
†These authors contributed equally.

https://doi.org/10.18494/SAM3740

are powered by a precharged battery with limited electric energy, making it difficult to ensure their long-term sustainable operation.[4] Owing to the widespread distribution of nodes, as many as 300 WSNs may need to be arranged in a 25 $m^2$ area,[5] making it difficult to ensure that all nodes have sufficient battery charge. Therefore, a new energy supply approach for WSNs is urgently required to overcome the energy limitation of precharged batteries.[6] An environmental energy harvesting technology is one possible approach.[7] Energy harvesting has been successfully applied to WSNs employed in transportation,[8] human activities,[9–11] outdoor solar generation,[12] and wind generation,[13] and it is becoming increasingly important for supporting the extended use of distributed IoT devices.[14,15]

Energy harvesting is also popular in grid applications.[16] Electromagnetic energy harvesting from power transmission lines can power WSNs to sustainably monitor the three-phase voltage, current, and other power quality parameters.[17] For typical IoT sensors with power consumption above 10 mW,[18] piezoelectric generators and triboelectric nanogenerators require a stable vibration power input and a large-area energy harvesting device,[19–22] which is not conducive to being arranged on the shell of a transformer, while solar energy harvesting is reliable for powering the WSN to monitor environmental quantities such as temperature, humidity, vibration, and illumination, which are also important indicators that reflect the operating conditions of a transformer.

Photovoltaic panels[23] are most commonly used in solar energy harvesting owing to their high efficiency, low cost, cleanliness, and easy access.[24] In outdoor applications, a photovoltaic panel can generate a high power of 15 mW/$cm^2$ with an efficiency of up to 30% on a sunny day.[25] However, little or no power is generated in the evening or at night, which together make up two-thirds of the 24 h day, or on cloudy or rainy days with weak light. Therefore, solar energy harvesting under weak lighting conditions should also be utilized to ensure a sustainable power supply.[26] The small area of photovoltaic panels that can be used for a WSN also limits the output power.

An energy management strategy involving a hybrid supercapacitor and lithium battery has been demonstrated to be effective in solar-powered systems, especially solar vehicles.[27] Many dynamic algorithms to optimize the energy management strategy have been proposed. Liu *et al.*[28] designed a sponge supercapacitor rule-based energy management strategy for WSNs, which was optimized using a dynamic programming algorithm. However, complex algorithms consume more power, making them less viable for small-scale energy harvesting.

To address these challenges in small-scale solar energy harvesting, many power management approaches have been utilized such as a low operation voltage,[29] low-dropout (LDO)[30] undervoltage lockout (UVLO),[31] and maximum power point tracking (MPPT).[32] Some commercial chips are recommended for harvesting weak solar energy such as LTC3105 (Linear Technology)[33] and BQ25504 (Texas Instruments).[34] Wu *et al.*[35] designed an IoT platform and autonomous WSN for environmental monitoring. Their power management circuit was based on an LTC3105 chip with a rechargeable battery as the energy storage device. However, the lifetime of autonomous operation in total darkness of 81 h shows that the service life of such a WSN still depends on the capacity of the energy storage elements. Vračar *et al.*[36] designed a telemetry node optimized for low illumination, using a 1.5 F supercapacitor as the standby energy storage

element. However, owing to the low energy harvesting level, the DC–DC converter was omitted and an electrolytic capacitor was used as a direct power supply. Although their node could stabilize a cold start, it could not provide a stable power supply voltage or ensure that the supercapacitor voltage rises to a sufficient level when there is light. Abella *et al*.[37] designed an energy-saving WSN platform using a battery as the only energy storage element, but did not consider the response time or the low conversion efficiency. The peak current output by the battery was only 10 mA, which may further decrease upon matching the high periodic pulse of WSN power consumption. These power management designs cannot effectively solve the balance between the fast start-up and continuous operation of a WSN in an environment with alternating strong and weak light.

In practical applications, WSNs consume a large amount of energy during data acquisition, processing, and communication,[38] and a direct solar power supply is difficult to stabilize to ensure the sustainable operation of WSNs. In particular, an environment with alternating strong and weak light[39] leads to an unstable solar power supply.[40] The power management circuit requires energy storage elements with sufficient capacity to deal with a working environment without an external energy input, such as at night, and the high energy storage capacity will inevitably lead to a long energy storage cycle, thus delaying the rapid start-up and reducing the responsiveness of WSNs.

To solve the above problems, we have designed a power management circuit with dual-stage energy storage comprising a supercapacitor and a lithium battery, and we propose an innovative design for dual-channel lithium battery charging with switching control according to the lighting conditions, as reported in this paper. The power management circuit can operate in four modes: direct power supply mode, supplementary discharge mode, low-power surplus charging mode, and high-power surplus charging mode. In the direct power supply mode, the photovoltaic energy is stored in the supercapacitor to quickly provide energy for the WSN. In the supplementary discharge mode, the illumination input is insufficient, and the WSN continues to be powered by the energy stored in the lithium battery. In the surplus charging modes, while the light input supplies power to the WSN through the supercapacitor, the surplus photovoltaic energy is stored in the lithium battery. The microcontroller of the WSN judges the light level and charges the lithium battery in two channels of low power and high power to supplement the consumption of the battery during discharge. The design can ensure a sustainable power supply and the effective utilization of photovoltaic energy.

We also designed a multifunctional WSN with low power consumption for temperature, humidity, vibration, and illumination monitoring in grid applications. By modeling and simulation of a solar-powered WSN in a whole system using LTspice, we determined and optimized the parameters and the logic used for power management. In an experiment on the solar-powered system, dual energy storage element charging curves of the supercapacitor and lithium battery were tested to verify the quick charging ability. The power management logic was also validated outdoors under different lighting conditions to verify the sustainability of the power supply to the WSN. The upper computer front panel for WSN autonomous monitoring was evaluated in a laboratory, and was shown to have potential use in grid transformer applications.

## 2. Overall Architecture of Power Management

The solar energy harvested in the actual environment is usually relatively weak and greatly affected by external factors, making it difficult to directly provide a stable and sufficient energy supply for sensor nodes and their functional modules, especially for sensor nodes that must switch between sleep, RF communication, and other working modes with large power consumption differences. The instability of environment energy harvesting and the changes in WSN power consumption often lead to a time mismatch between energy harvesting power and WSN consumption power.[41] In serious cases, packet loss or even power loss occurs during node data transmission. This mismatch between environmental energy intake and node energy consumption in terms of the time and total amount imposes requirements on the design of power management circuits.

A general power management circuit is composed of functional links such as for energy harvesting, energy conversion, energy storage, and power supply.[42] An innovative photovoltaic energy harvesting power management circuit must take into account the WSN energy demand in an environment with alternately strong and weak lighting, and ensure that the energy storage elements at all levels can be effectively charged after power consumption. In this paper, we propose the power management circuit design of a supercapacitor and lithium battery dual energy storage with dual-channel charging of the lithium battery, whose overall architecture is shown in Fig. 1.

As shown in Fig. 1, the solar energy harvesting unit is a photovoltaic panel. To meet the requirements of high pulse power consumption and long-term standby for WSNs, a supercapacitor with high power density and long cycle life is used as the first energy storage unit, and a lithium battery with high energy density and stable voltage is used as the second energy storage unit. The supercapacitor has ideal power density and energy density characteristics. It can not only store enough energy to support the operation of the node for a considerable period of time but also provide high pulse power. Owing to its unlimited charge and discharge times and high charge and discharge efficiency, it is very suitable for application to self-powered WSNs. However, the existence of leakage current limits its long-term energy

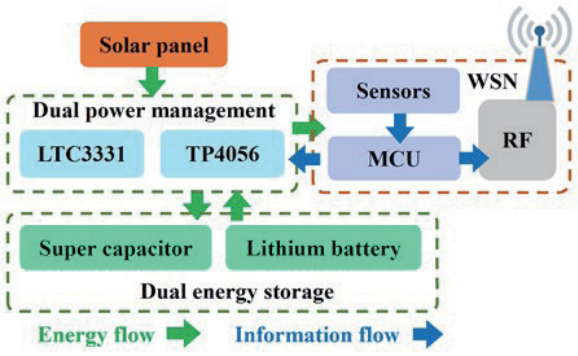


Fig. 1. (Color online) Overall architecture of dual-channel power management in WSN powered by solar energy harvesting.

storage capacity. It is therefore used in combination with rechargeable lithium batteries, which have the advantages of high energy density and low leakage, to provide high pulse power, a short start-up time, and the long-term storage of standby energy.

To deal with different charging currents of photovoltaic power generation under strong and weak light illumination, an LTC3331 dual-channel power management chip and a TP4056 lithium battery dedicated fast charging chip are used as the lithium battery charging circuit. The LTC3331 chip[43] is an energy harvesting power management chip that provides an input interface for the original DC output of the photovoltaic panel and stores the electric energy in the supercapacitor. It can also charge the battery with a low current charging capacity of 0–10 mA when there is excess input solar energy for the supercapacitor. In contrast, the TP4056 lithium battery charging chip[44] has a current charging capacity of 10–1000 mA for the battery with a charge and discharge protection function. The DC-DC converter of the dual power management chips provides a stable power supply voltage for the WSN. In addition to data acquisition, processing, and transmission, the microcontroller unit (MCU) of the WSN also monitors the ambient lighting conditions and controls the dual energy storage strategy accordingly. The working mode and workflow of the circuit are shown in Fig. 2.

As shown in Fig. 2, the input energy of the photovoltaic cell first passes through a full bridge rectifier circuit and a UVLO circuit. The rectifier bridge can prevent a countercurrent. The UVLO circuit disconnects the rear stage circuit and stores the energy in the supercapacitor. When the supercapacitor voltage rises to the hysteresis window threshold $V_{rise}$, the rear stage path is opened. Through the buck converter circuit, the WSN is powered by a small-capacity electrolytic capacitor $C_{out}$, which stabilizes and filters the voltage. A flowchart of the dual-channel energy path control process is shown in Fig. 3 and the specific circuit design is discussed in Sect. 4. Our proposed power management circuit has four modes as follows:

(1) Direct power supply mode: the voltage $V_{cin}$ of the supercapacitor of the primary energy storage element is between the UVLO rising threshold $V_{rise}$ and the falling threshold $V_{fall}$, the photovoltaic energy stored by the supercapacitor directly supplies power to the WSN through the buck converter, and the lithium battery charge and discharge circuits are closed.

(2) Battery power supply mode: $V_{cin}$ is less than $V_{fall}$ due to a lack of light, such as on rainy days and at night, the buck-boost converter of the LTC3331 power management chip is turned on,

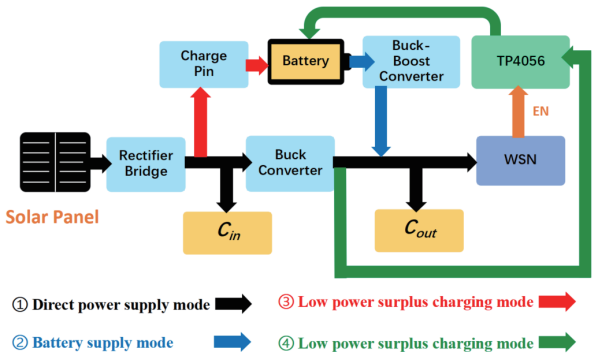


Fig. 2. (Color online) Workflow of dual-channel power management.

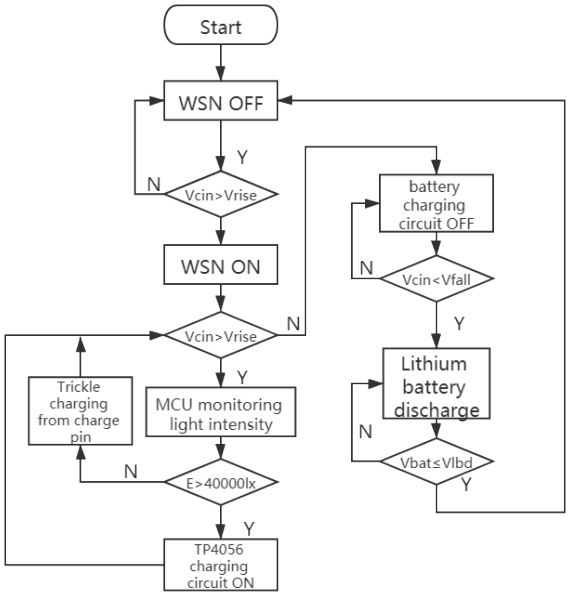


Fig. 3. Energy path control flowchart.

and the lithium battery used as the secondary energy storage element supplies power to the WSN.

(3) Low-power surplus charging mode: the MCU of the WSN obtains the ambient illumination through the illumination sensor while it is in operation. The illumination threshold of the TP4056 lithium battery charging circuit is 40000 lx, which is also the illumination value used under the standard test conditions of photovoltaic panels. When the photovoltaic input causes $V_{cin}$ to exceed $V_{rise}$, if the ambient illumination $E$ does not reach 40000 lx, the MCU outputs a high-level signal to the metal oxide semiconductor (MOS) gate through the input/output (IO) port to turn it off. At this time, the LTC3331 chip slowly charges the lithium battery through its charge pin.

(4) High-power surplus charging mode: the illuminance is higher than 40000 lx, indicating that the illumination is sufficient to quickly charge the lithium battery while maintaining the operation of the WSN. The MCU outputs a low-level signal to turn on the MOS gate. The energy output by the solar panel flows to the lithium battery through the high-power charging channel provided by the TP4056 chip dedicated to the fast charging of the lithium battery to improve the charging speed of the lithium battery while the LTC3331 chip still charges the lithium battery.

## 3. Environmental Monitoring WSN Design

### 3.1 Multifunctional WSN design

Transformer environmental monitoring includes temperature, humidity, and vibration monitoring. Changes in the ambient temperature cause heating and cooling anomalies in the

windings and affect oil temperature measurement. Humidity affects the cooling state of the equipment. Vibration characteristics reflect a variety of problems, including short-circuiting, winding breaks, overpressure, and overcurrent. Therefore, in addition to monitoring transformer electrical parameters, environmental parameter monitoring is also indispensable.

To meet the need for transformer environmental monitoring, we have designed a low-power multifunctional WSN using the very low power ATmega328P microcontroller as the main control unit. The sensing unit of the WSN uses a DHT22 integrated temperature and humidity sensor and an ADXL345 three-axis vibration sensor. A BH1750FVI light sensor is also added to monitor light for dual-channel power management. The multifunctional WSN for monitoring transformers operating under abnormal conditions can measure vibration in the range of ±16 g and has a sensitivity of 3.9 mg/LSB, a temperature measurement range from −40 to 80 ℃ with a resolution of 0.1 ℃, and a humidity measurement range from 0 to 100 %RH with a resolution of 0.1% RH.

The wireless transceiver of the WSN uses an NRF24L01+ module based on enhanced ShockBurst protocol, where the microcontroller converts the data read by the sensors into single-precision floating points and hexadecimal according to the IEEE 754 floating-point calculation standard. As the humidity, temperature, *x*-axis vibration, *y*-axis vibration, *z*-axis vibration, and battery voltage are sequenced into the sending load register and packaged for transmission, the data are received by the upper receiver and displayed on the upper computer in real time. A working diagram of the WSN is shown in Fig. 4.

### 3.2 Low-power-consumption design of WSN

There is a mismatch between the unstable and low solar energy harvesting power and the high power consumption required for the WSN to collect and send data. To solve this problem, in addition to configuring dual energy storage links on the hardware circuit, it is also important to control the WSN operation duty via software. The WSN operating cycle can be divided into a high-power operating state and a very low power sleep state, giving it the power consumption characteristics of periodic pulses. The energy storage element provides sufficient power for data

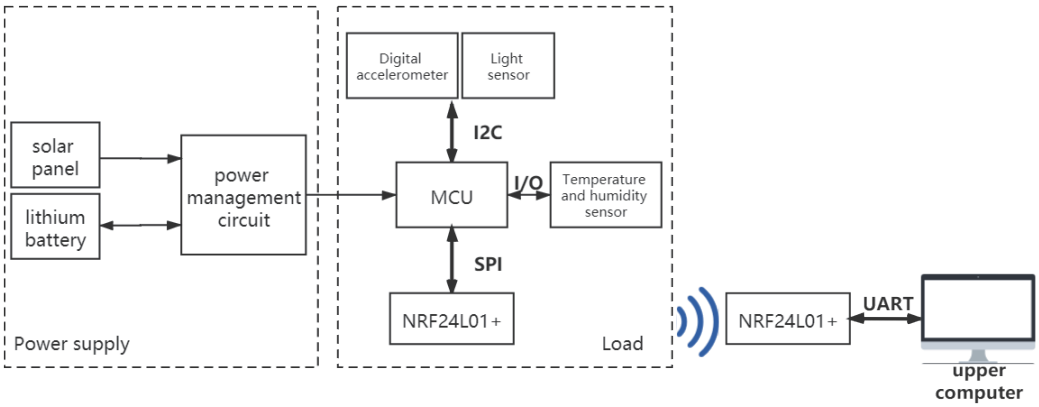


Fig. 4. (Color online) Working diagram of WSN.

transmission when the WSN enters the operating state. This overcomes the conflict between the power characteristics of the energy harvester and the WSN, thus realizing a stable sustainable self-power supply and autonomous monitoring.

The ATmega328P processor supports six low-power modes to reduce consumption by shutting down the function modules not in use, where the power-down mode consumes the least power among the modes. In this design, four bits (0101) are written to the slave mode control register to put the WSN into power-down mode. The WSN is then woken up after a certain period of time through a watchdog interruption. After entering the power-down mode, the external oscillator stops working and only the external interrupter and the watchdog keep working. The consumption current can be as low as 0.36 mA. The sleep time depends on the charging time of the energy storage element. To avoid the operating state of the WSN triggering UVLO falling, the energy stored by the energy storage element during the sleep time should reach a sufficiently high level. In the power management circuit design, the WSN is set to work for 10 s in a cycle and sleep for 1 min. The workflow of the WSN in the low-power mode is shown in Fig. 5.

### 3.3 WSN power consumption test

An LPA375 low-power analyzer is used to test and compare the power consumption curves of the WSN in the normal mode and low-power mode. The power consumption curves are analyzed using Otii power consumption test software. As shown in Fig. 6(a), in the normal mode, the WSN consumes an average current of 18.9 mA under a 4.5 V supply voltage. Such a high power

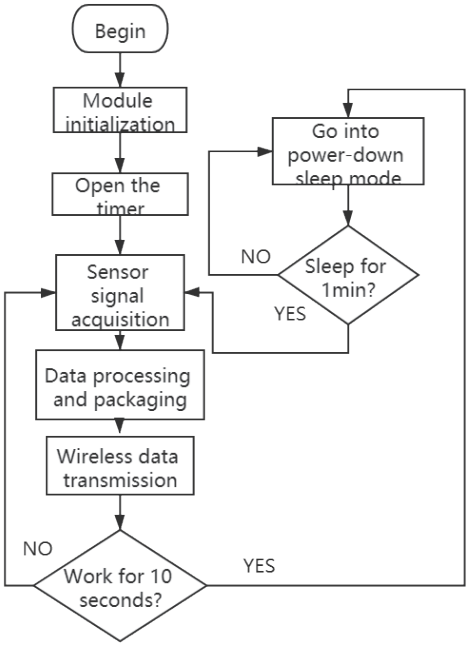


Fig. 5. Low-power-mode workflow.

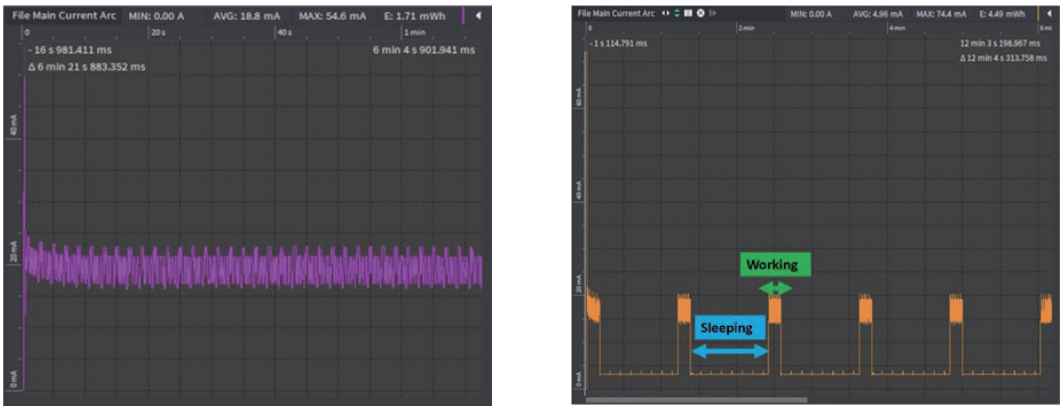


(a) (b)

Fig. 6. (Color online) Comparison of WSN power consumption curves. (a) Normal mode and (b) low-power mode.

consumption of 85.05 mW is not conducive to energy harvesting, and the system cannot easily store excess power. However, after low-duty-cycle programming, the average current consumed is only 4.96 mA, reducing the overall power consumption by about 73.6%. Thus, the low-power design of the WSN is effective, making a major contribution to realizing the self-power supply of the system.

## 4. Design of Solar Power Management Circuit

### 4.1 MPPT design of the photovoltaic cell

A polysilicon photovoltaic panel with an area of 105 × 66 $mm^2$ is chosen as the solar energy harvesting unit. The output characteristic curves of the photovoltaic cell are measured at 2:00 p.m. on a sunny day.

As shown in Fig. 7, the photovoltaic cell generates a high power between 4 and 6 V, making it a suitable energy harvesting source for power management circuits. According to the principle of the open-circuit voltage method in photovoltaic MPPT,[45] the ratio of the maximum power point voltage to the open-circuit voltage is usually between 0.71 and 0.78. Therefore, when designing the circuit, keeping the output voltage of the photovoltaic cell within this range can realize an output near the maximum power. Although this method has low accuracy and does not consider the influence of temperature changes on the maximum power point, it does not need a complex control circuit and can reduce the cost and the power consumed by the MCU tracking calculation.

### 4.2 Power management design of dual energy storage element

The LTC3331 chip has a full bridge rectifier and a buck converter circuit with an input range of 3 to 19 V, which is sufficient for solar energy harvesting applications. The input side is

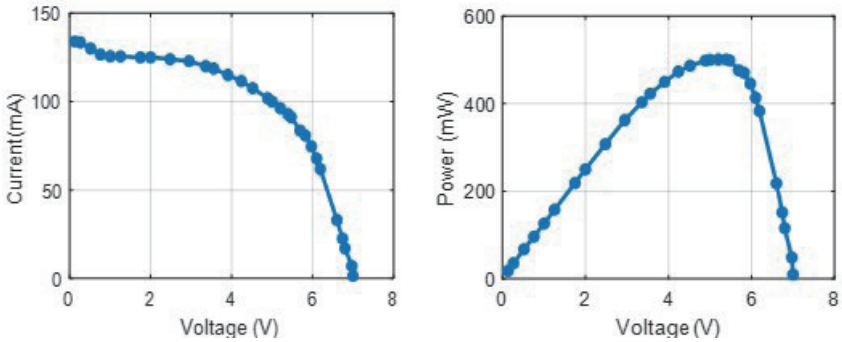


Fig. 7. (Color online) Output characteristic curves of the photovoltaic cell. (a) *I–V* curve and (b) *P–V* curve.

controlled by a UVLO that can be programmed by the pin logic input. By configuring the high and low levels of the pin, the UVLO can control the input voltage to near the MPPT voltage of the energy harvesting source. On the basis of the high power range of the photovoltaic cell measured in Fig. 7, a UVLO range of 4–5 V is chosen in the LTC3331 circuit design. Controlling the UVLO consumes a static current of only 450 nA; thus, low-power energy harvesting sources can efficiently store energy in the input supercapacitor, the primary energy storage element.

When the voltage of the primary energy storage element first reaches the UVLO rising threshold of 5 V, the buck converter turns on with a very low quiescence current and outputs a stable voltage of 3.3 V to power the WSN until the voltage falls to the UVLO falling threshold of 4 V.

If the voltage of the primary energy storage element rises above the UVLO rising threshold of 5 V, a shunt starts charging the second energy storage element, which is a lithium battery, through a charging pin. If the voltage of the primary energy storage element drops below the UVLO falling threshold of 4 V, the buck converter is switched off, the boost converter is turned on, and the battery powers the WSN. An internal PMOS switch is disconnected to protect the battery from damage during over-release.

A supercapacitor with a capacity of 330 mF and a withstand voltage of 7.5 V is selected as the primary energy storage element. A 602030 model lithium battery with a capacity of 300 mAh and a nominal voltage of 3.7 V is selected as the second energy storage element in the power management circuit design. According to the average current consumption in the low-power mode shown in Fig. 6, the WSN can operate continuously in a dark environment for approximately 76 h when the battery is fully charged.

To verify the logic of the self-powered system, a system model including the LTC3331 power management circuit model and WSN time-varying load model is established in LTspice, and the time-varying curves of the input and output voltages are obtained through simulation. As shown in Fig. 8, the input voltage first rises quickly and provides a regulated output for the WSN after it reaches 5 V, then it fluctuates between 4 and 6 V as the power consumption of the WSN alternates. When the input voltage is above 5 V, the circuit starts to charge the battery while simultaneously supplying power to the WSN.

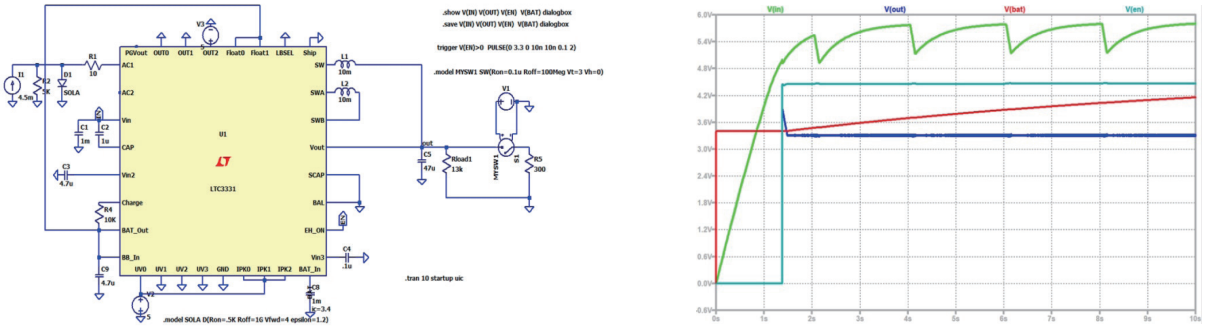


(a) (b)

Fig. 8. (Color online) Model and simulation of LTC3331 circuit. (a) LTspice model of LTC3331 circuit and (b) simulation curve of LTC3331 circuit.

### 4.3 Design of dual-channel battery charging circuit

The LTC3331 power management chip has a lithium battery charging function that charges a lithium battery when the supercapacitor voltage is above the UVLO rising threshold. On the basis of the chip data sheet, its charging current is determined as

$$I_{charge} = \frac{4.8V - V_{LBD}}{R_{charge} + 60}. \tag{1}$$

$I_{charge}$: charging current (A)
$V_{LBD}$: low-battery disconnect (V)
$R_{charge}$: charging pin current limit resistance (Ω)

In the chip design, $V_{LBD}$ is 2.7 V, and to maximize the battery charging current, we short the resistor $R_{charge}$ to reach the theoretical maximum charging current of 35 mA. However, owing to a shunt current limitation, the measured lithium battery charging current is only 1.7 mA. Assuming that solar energy harvesting is available for 13 h from 6:00 a.m. to 7:00 p.m. on a sunny day, the shunt in the LTC3331 chip can charge the lithium battery during this time. In the remaining 11 h without solar energy harvesting, the WSN is powered by the lithium battery. Assuming that the lithium battery is linearly charged and discharged, we roughly estimate the charging energy input to the battery and its discharging energy in 24 h to be about $1.7\ \text{mA} \times 13\ \text{h} = 22.1\ \text{mAh}$ and $4.96\,\text{mA} \times 11\ \text{h} = 54.56\ \text{mAh}$, respectively. Because the discharging energy is greater than the charging energy, the energy in the lithium battery will gradually be consumed, and the WSN is unsustainable. Therefore, another lithium battery charging circuit must be designed to provide a higher charging current to the lithium battery when the light is sufficient. When the light is insufficient, the lithium battery still supplies power to the WSN through the buck-boost converter of the LTC3331 chip.

The improved dual-channel lithium battery circuit uses a TP4056 integrated chip to build a high-speed charging path for the lithium batteries. The classic TP4056 low-cost lithium battery

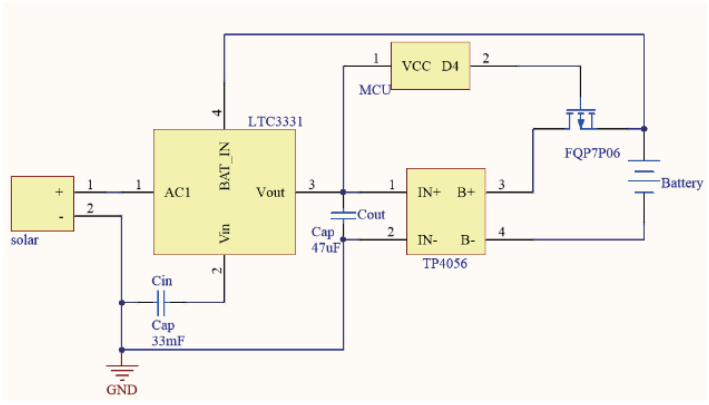


Fig. 9. (Color online) Dual-channel lithium battery charging circuit.

charging chip provides a stable charging voltage of 4.2 V and a charging current of up to 1 A. It also integrates a DW01 battery protection chip and a 8205A dual MOS power tube on the charging side to protect the lithium battery from overcharging and overdischarging.

The charging path of the TP4056 chip is controlled by the MCU, and an FQP7P06 P-channel-enhanced MOS tube is used as a circuit switch in this design. The ambient lighting is detected by a BH1750FVI light sensor for switching control. The connection diagram of the dual-channel lithium battery charging circuit is shown in Fig. 9.

To determine a light threshold as the condition for charging path switching control, the illumination from 6:00 a.m. to 8:00 p.m. and the voltage of the solar cell during this time were measured on a June day at a temperature between 21 and 35 °C. As shown in Fig. 10, the photovoltaic cell maintains a voltage of higher than 4 V between 6:00 a.m. and 7:00 p.m., providing continuous energy to the WSN, and the lithium battery can power the WSN during the remaining 11 h. If a condition of illumination higher than 40000 lx for the opening of the TP4056 charging path is set, then the path will be continuously open for about 6 h a day to charge the lithium battery. From the battery consumption of 54.56 mAh calculated above, the TP4056 charging current must be at least 9 mA to replenish the lithium battery and make the WSN sustainable.

## 5. Test of Solar-powered System

### 5.1 Test of energy storage element charging

(1) Supercapacitor charging test

The charging speed of the supercapacitor mainly depends on the photovoltaic cell's output power and the efficiency of the power management circuit. Figure 11 shows the measured supercapacitor voltage charging curve. The supercapacitor voltage reaches the UVLO rising threshold of 5 V in 30 s when the illumination is sufficient, which indicates that the WSN has a start-up. The average charging power before the voltage reaches 5 V is $0.5 \times 0.33\ \mathrm{F} \times 5\ \mathrm{V} \times 5\ \mathrm{V} / 13.7\ \mathrm{s} = 301.09\ \mathrm{mW}$.

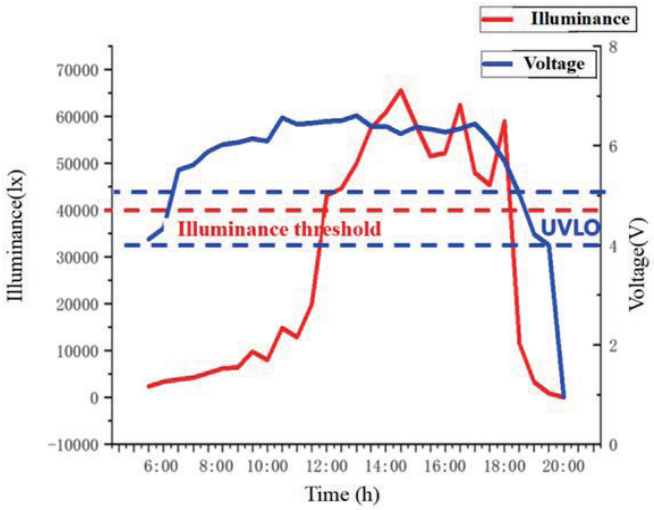


Fig. 10. (Color online) Sunlight and photovoltaic voltage during the day.

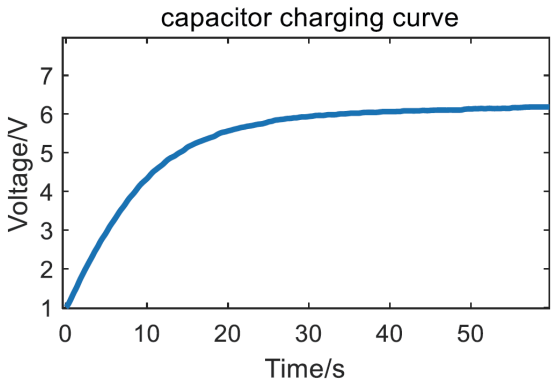


Fig. 11. (Color online) Supercapacitor charging curve.

(2) Lithium battery charging test

The power management circuit has different charging currents in the low-power surplus charging mode and high-power surplus charging mode. We used the resistor divider method to measure the charging currents. A small resistance of 1 Ω was added to the lithium battery charging circuit in series, and the voltage across the resistance was read by a multimeter so that the charging currents could be calculated using Ohm's law. The charging currents of the low-power surplus charging mode and high-power surplus charging mode are shown in Table 1.

In the high-power surplus charging mode, the lowest charging current is 9 mA and the maximum current is 20.2 mA, thus providing sufficient energy for the lithium battery. The power curves of the lithium battery over 24 h when it is charged with and without dual channels are shown in Fig. 12. If only the LTC3331 chip is used for lithium battery charging, the total power of the battery drops after 21 h and eventually runs out. However, when the TP4056 chip is added to form a two-channel charge, the battery can make up for its losses and even store surplus power generated during the day.

Table 1
Lithium battery charging currents.

| | Low-power surplus charging mode | High-power surplus charging mode |
|---|---|---|
| Charging current (mA) | 1.7 | 9–20.2 |

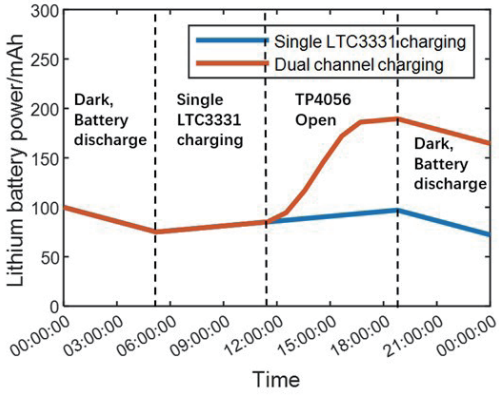


Fig. 12. (Color online) Lithium battery power curves over 24 h.

## 5.2 Verification of power management logic

To verify the logic of the dual-channel power management design, the supercapacitor voltage curves under different lighting conditions and power supply modes are measured and observed using an oscilloscope. The supercapacitor voltage curves and output voltage curves under different lighting conditions are shown in Fig. 13.

The photovoltaic output power is very high on sunny days. The $V_{out}$ pin of the LTC3331 chip immediately outputs a voltage of 4.5 V when the capacitive voltage rises to 5 V, and the WSN is powered on and remains stable. When the WSN is operating, the charging curve slope is low but continuously rises, and the voltage increases quickly and can reach up to 6 V when the WSN sleeps.

On cloudy days, the measured capacitor charging speed is lower than that on sunny days, and the capacitive voltage is significantly reduced when the WSN is powered on. Then, within 1 min of the WSN entering sleep mode, the capacitive voltage slowly rises to about 5.36 V, then quickly drops to about 4.72 V when the WSN is woken. The capacitive voltage then stably remains between these two values, i.e., within the optimal power generation range of the photovoltaic cell, indicating full use of the photovoltaic power harvesting.

In the lightless environment, the measured supercapacitor voltage gradually drops. When it reaches 4 V, the voltage of the EH_ON pin of the LTC3331 chip jumps to a low level, indicating that the energy harvesting power supply has switched to battery power, while the output voltage remains stable at about 4.5 V and the WSN continues to operate stably. The above tests verified the validity of the dual energy storage element design.

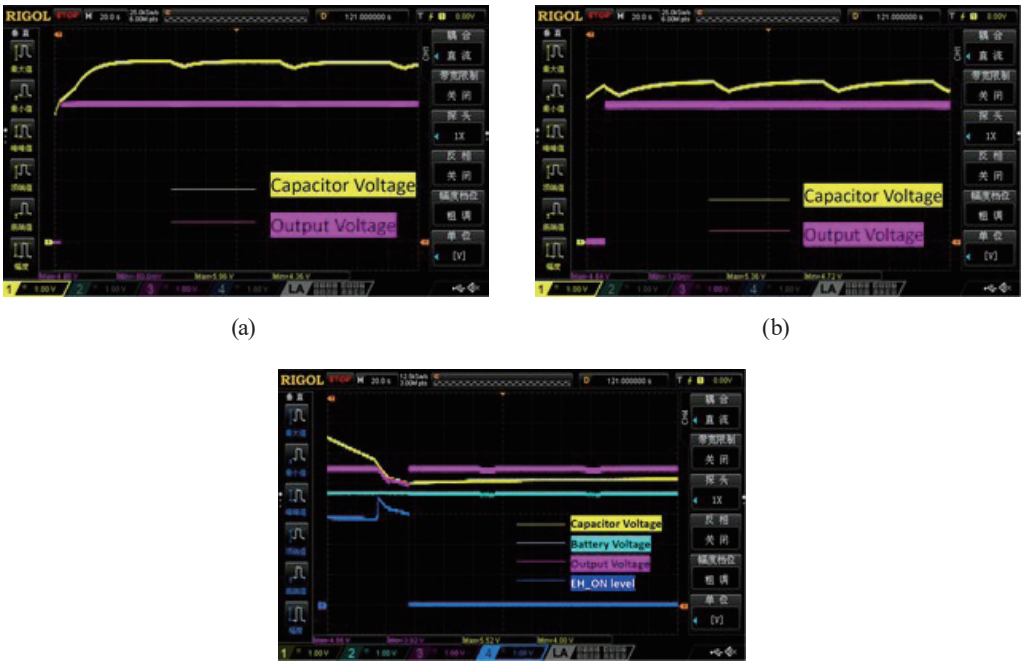


Fig. 13. (Color online) Voltage curves under different lighting conditions. (a) Sufficient light on sunny days, high-power surplus charging mode. (b) Weak light on cloudy days, low-power surplus charging mode. (c) No light, WSN powered by lithium battery, supplementary discharge mode.

### 5.3 Solar-powered wireless sensing system

To visualize and monitor WSN acquisition data in real time, an upper computer front panel was written in Labview2018 as shown in Fig. 14. An NRF24L01+ receiver module is connected to the computer via a serial port, which receives data from the WSN wirelessly and sends the data to the computer for processing and display via serial communication. The front panel can monitor the temperature, humidity, and vibration data and the battery level received by the WSN in real time, and can store the historical data as CSV files. In addition, the upper computer can directly collect the three-axis vibration data of the WSN for Fourier spectrum analysis. The upper computer can also detect anomalies in the temperature, humidity, or vibration signal of the monitored transformer and provide an alarm.

When the transformer is operating normally, the vibration base frequency is around 100 Hz. In a laboratory experiment, whose setup is shown in Fig. 15, a vibration signal of 100 Hz is generated with a JDS6600 signal generator, and the ADXL345 sensor of the WSN is pasted onto an E-JZK-10 vibration exciter. The vibration amplitude is adjusted to 0.5, 1, or 1.5 g via an SA-PA010 power amplifier. The exciter generates vibration along the *z*-axis of the sensor, and the WSN wirelessly transmits the vibration data to the receiver. The frequency domain information of the vibration displayed by the upper computer is shown in Fig. 16. The upper computer front

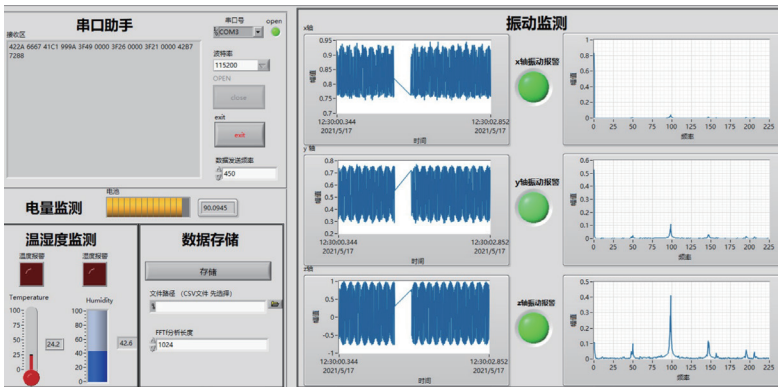


Fig. 14. (Color online) Upper computer front panel.

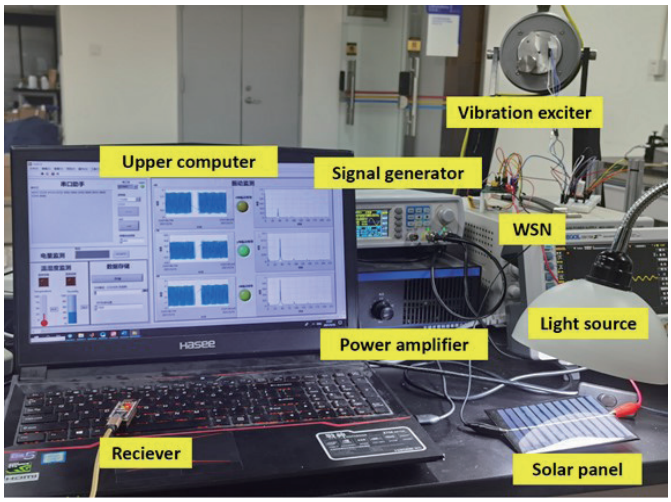


Fig. 15. (Color online) Experimental setup.

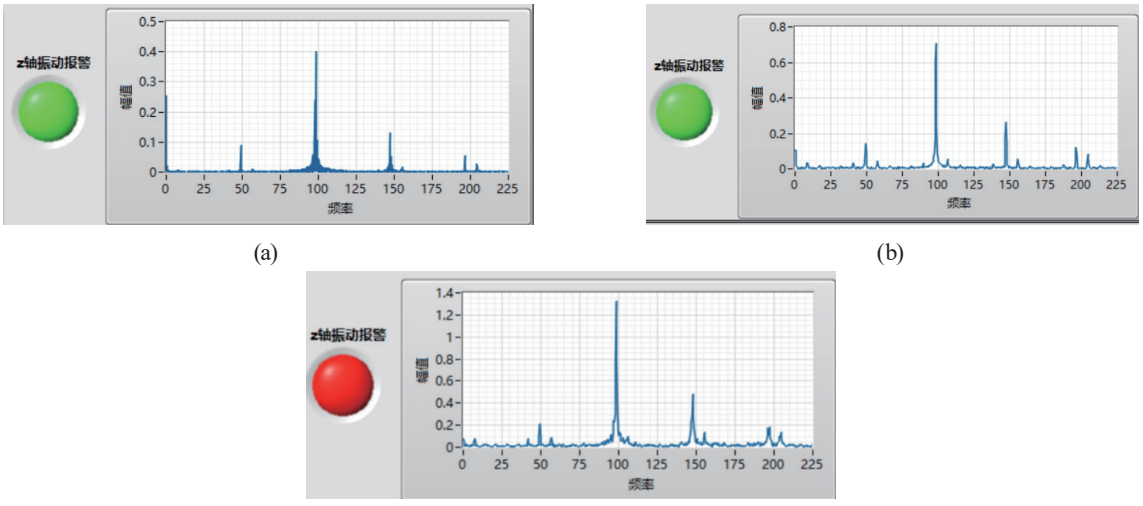


Fig. 16. (Color online) Demonstration of monitoring by upper computer showing spectra for 100 Hz vibration with amplitudes of (a) 0.5 g, (b) 1 g, and (c) 1.5 g.

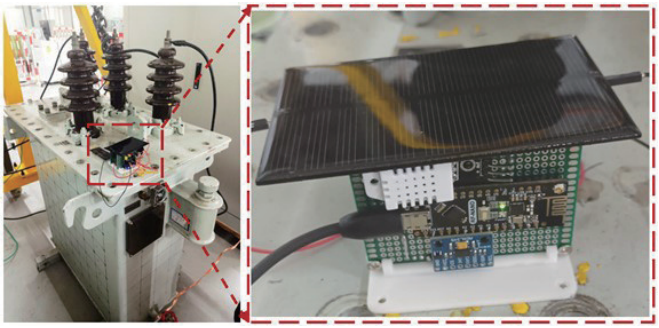

Fig. 17. (Color online) Solar-powered WSN in grid transformer application.

panel can accurately identify the vibration frequency. When the amplitude exceeds 1 g, the vibration alarm indicator turns red to sound an alarm. The deviation in the amplitude measurement may be due to the sub-optimal installation location of the sensor or the low thickness of the sensor PCB plate. Similarly, the upper computer sounds an alarm when the temperature exceeds 40 °C or the humidity exceeds 60% RH.

The above experiment demonstrates sustainable and autonomous wireless sensing by the designed dual-channel charging and dual storage elements during solar energy harvesting. The solar-powered WSN designed in this study is promising for use in grid transformer applications as shown in Fig. 17.

## 6. Conclusions

Multifunctional WSNs for sensing and state monitoring play an important role in the development of intelligent manufacturing and the industrial IoT, and energy harvesting is a key approach to address the energy limitations of WSNs and ensure sustainable autonomous applications. On the basis of the wireless environmental monitoring application in grid transformers, we designed a solar-powered WSN and its power management circuits. The power management circuits of the dual energy storage elements and dual-channel lithium battery responded to changes in the light characteristics. This design balances the requirements of a fast start and an energy reserve for the WSN, provides trickle charging and relatively fast charging, and guarantees that the energy consumed by lithium batteries can be replenished to achieve long-term sustainable operation. To achieve low power consumption, the WSN operates for 10 s then sleeps for 1 min in one cycle, i.e., the duty cycle is 14.3%, and the average current consumption is 4.96 mA. The solar-powered WSN can quickly start in less than 30 s from an empty energy state, and the lithium battery charging current has a maximum of 20.2 mA and a minimum of 1.7 mA. Our proposed design achieves stable dual-channel lithium battery charging and can provide sustainable power supply to a WSN.

## Acknowledgments

This work was supported in part by the National Natural Science Foundation of China (Grant Nos. 51890884), Jiangsu Province Foreign Expert Program (Grant No. BX2020032), the

Recruitment Program of Global Experts (Grant No. WQ2017610445), and the 111 Program (Grant No. B12016). Data supporting the findings of this study are available from the corresponding author upon reasonable request.

## References


1 A. J. Christina, M. A. Salam, and Q. M. Rahman: Renewable Sustainable Energy Rev. **82** (2018) 1442. https://doi.org/10.1016/j.rser.2017.05.165
2 L. Liu, X. Guo, and C. Lee: Nano Energy **88** (2021) 106304. https://doi.org/10.1016/j.nanoen.2021.106304
3 S. S Reka and T. Dragicevic: Renewable Sustainable Energy Rev. **91** (2018) 90. https://doi.org/10.1016/j.rser.2018.03.089
4 N. Qi, K. Dai, F. Yi, and X. Wang: IEEE Access **7** (2019) 88289. https://doi.org/10.1109/ACCESS.2019.2919986
5 M. Rossi, L. Rizzon, and M. Fait: IEEE J. Emerging Sel. Top. Circuits Syst. **4** (2014) 324. https://doi.org/10.1109/JETCAS.2014.2337171
6 F. K. Shaikh and S. Zeadally: Renewable Sustainable Energy Rev. **55** (2016) 1041. https://doi.org/10.1016/j.rser.2015.11.010
7 X. Tang, X. Wang, and R. Cattley: Sensors **18** (2018) 12. https://doi.org/10.3390/s18124113
8 M. Gao, J. Cong, and J. Xiao: Appl. Energy **257** (2020) 113969.1. https://doi.org/10.1016/j.apenergy.2019.113969
9 Z. Yang, B. Lin, and L. Zhou: Fundam. Res. (2021). https://doi.org/10.1016/j.fmre.2021.05.002
10 T. He and C. Lee: IEEE Open J. Circuits Syst. **2** (2021) 702. https://doi.org/10.1109/OJCAS.2021.3123272
11 T. He, X. Guo, and C. Lee: iScience **24** (2021) 101934. https://doi.org/10.1016/j.isci.2020.101934
12 J. Silva-Leon, A. Cioncolini, and M. R. A. Nabawy: Appl. Energy **239** (2019) 846. https://doi.org/10.1016/j.apenergy.2019.01.246
13 Y. Tan, G. Lu, and M. Cong: Energy Convers. Manage. 238. (2021). https://doi.org/10.1016/j.enconman.2021.114173
14 J. Zhu, X. Liu, and Q. Shi: Micromachines **11** (2020) 7. https://doi.org/10.3390/mi11010007
15 Z. Ren, J. Xu, and X. Le: Micromachines **12** (2021) 946. https://doi.org/10.3390/mi12080946
16 H. E. Erdem and V. C. Gungor: Ad Hoc Networks **75–76** (2018) 98. https://doi.org/10.1016/j.adhoc.2018.03.002
17 O. Menénde, S. Kouro, and M. Pérez: AEU Int. J. Electron. Commun. **110** (2019) 152830. https://doi.org/10.1016/j.aeue.2019.152830
18 S. A. Afghan and H. Géza: Energies **12** (2019) 3873. https://doi.org/10.3390/en12203873
19 M. Zhu, M. Zhu, and Z. Yi: Nano Today **26** (2021) 101016. https://doi.org/10.1016/j.nantod.2020.101016
20 H. Wang, J. Zhu, and T. He: Nano Energy **78** (2020) 105241. https://doi.org/10.1016/j.nanoen.2020.105241
21 L. Liu, B Yang, and Y. Zhai: Nano Energy **76** (2020) 105052. https://doi.org /10.1016/j.nanoen.2020.104966
22 H. Liu, H. Fu, and L. Sun: Renewable Sustainable Energy **137** (2021) 110473. https://doi.org/10.1016/j.rser.2020.110473
23 W. Ma, X. Li, and H. Lu: Nano Energy **65** (2019) 104082. https://doi.org/10.1016/j.nanoen.2019.104082
24 A. A. F. Husain, W. Z. W. Hasan, and S. Shafie: Renewable Sustainable Energy Rev. **94** (2018) 779. https://doi.org/10.1016/j.rser.2018.06.031
25 H. Sharma, A. Haque, and Z. A. Jaffery: J. Renewable Sustainable Energy **10** (2018) 023704. https://doi.org/10.1063/1.5006619
26 L. Xie, W. Song, and J. Ge: Nano Energy **82** (2021) 105770. https://doi.org/10.1016/j.nanoen.2021.105770
27 Z. Cabrane, D. Batool, and J. Kim: J. Energy Storage **32** (2020) 101943. https://doi.org/10.1016/j.est.2020.101943
28 X. Liu, N. Qi, and K. Dai: Energy **19** (2021) 122368. https://doi.org/10.1016/j.energy.2021.122368
29 D. Newell and M. Duffy: IEEE Trans. Power Electron. **34** (2019) 9794. https://doi.org/10.1109/TPEL.2019.2894465
30 S. Mondal and R. Paily: IEEE Internet Things J. **4** (2017) 1624. https://doi.org/10.1109/JIOT.2017.2692383
31 P. Dorsch, T. Bartsch, and F. Hubert: Sensors **19** (2019) 1330. https://doi.org/10.3390/s19061330
32 F. F. Ahmad, C. Ghenai, and M. Bettayeb: Sustainable Energy Technol. Assess. **47** (2021) 101430. https://doi.org/10.1016/j.seta.2021.101430
33 Analog Institution: https://www.analog.com/en/products/ltc3105.html (accessed May 2021).
34 Ti Institution: https://www.ti.com.cn/product/cn/BQ25504 (accessed May 2021).
35 F. Wu, C. Rudiger, and M. R. Yuce: Proc. 2017 27th Int. Telecommunication Networks and Applications Conf. (IEEE, 2017) 1–6.
36 L. Vračar, A. Prijić, and D. Nešić: Electronics **5** (2016) 26. https://doi.org/10.3390/electronics5020026
37 C. S. Abella, S. Bonina, and A. Cucuccio: IEEE Sens. J. **19** (2019) 3501. https://doi.org/10.1109/JSEN.2019.2892604

38 L. Wang, T. He, and Z. Zhang: Nano Energy **80** (2021) 105555. https://doi.org/10.1016/j.nanoen.2020.105555
39 D. Yang, Y. Ni, and H. Su: Nano Energy **79** (2021) 105394. https://doi.org/10.1016/j.nanoen.2020.105394
40 E. Kabir, P. Kumar, and S. Kumar: Renewable Sustainable Energy Rev. **82** (2018) 894. https://doi.org/10.1016/j.rser.2017.09.094
41 Z. J. Chew, T. Ruan, and M. Zhu: IEEE Trans. Power Electron. **34** (2018) 8671. https://doi.org/10.1109/TPEL.2018.2885827
42 S. Zeadally, F. K. Shaikh, and A. Talpur: Renewable Sustainable Energy Rev. **128** (2020) 109901. https://doi.org/10.1016/j.rser.2020.109901
43 Analog Institution: https://www.analog.com/en/products/ltc3331.html (accessed May 2021).
44 Ysjianzhan Institution: http://proecb478.pic1.ysjianzhan.cn/upload/TP4056_datasheet.pdf (accessed May 2021).
45 S. H. Hanzaei, S. A. Gorji, and M. Ektesabi: IEEE Access **8** (2020) 182229. https://doi.org/10.1109/ACCESS.2020.3028580

## About the Authors

**Lu Wang** received his B.S. degree in mechanical engineering and automation in 2013 and his Ph.D. degree in 2021, both from Xi'an Jiaotong University. The Ph.D. degree included one year as a visiting student at the National University of Singapore. His research interests include energy harvesting, MEMS sensors and actuators, and structural vibration.

**Dongsheng Li** received his B.S. degree in instrument science and technology from Xi'an Jiaotong University in 2021. His research interests are solar energy harvesters and self-powered sensors.

**Yintao Ma** was born in Henan, China, in 1996. He received his B.S. degree in measurement and control technology and instruments from Sichuan University in 2018. In the same year, he joined Xi'an Jiaotong university as a graduate student. His research interests include atomic magnetometer, and MEMS/NEMS technology.

**Libo Zhao** was born in Yantai, China, in 1978. He received his M.S. and Ph.D. degrees in instrument science and technology in 2003 and 2007, respectively, both from Xi'an Jiaotong University, Xi'an, China. He is currently working as an associate professor in Xi'an Jiaotong University. His research interests include micro- and nanofabrication technology, MEMS sensor technology, and precision machining technology.

**Yao Chen** is an assistant professor of Xi'an Jiaotong University and is from the Department of Mechanical Engineering. His research areas include chip-scale atomic devices such as atomic magnetometers and atomic spin gyroscopes. He received his B.S. degree in the field of applied physics in 2009 from Beihang University. He received his PhD degree in the field of precision instrumentation and mechanical engineering in 2017 also from Beihang University. From 2017 to 2019, he was a postdoctoral researcher in the Physics Department of Harvard University. He is interested in quantum precision measurement based on trapped ions.

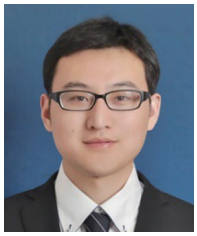

**Junlong Zhang** is currently a staff member of the International Joint Laboratory for Micro/Nano Manufacturing and Measurement Technologies and the School of Mechanical Engineering, Xi'an Jiaotong University (XJTU), China. He received his MSc degree from Okayama University, Japan.

**Zhuangde Jiang**, Ph.D, is a professor of Xi'an Jiaotong University and an academician of the Chinese Academy of Engineering. He is currently the director of the Institute of Precision Engineering (IPE), the vice director of the Chinese Society of Micro-Nano Technology (CSMNT), and the executive director of the Chinese Mechanical Engineering Society (CMES). His research areas include micro- and nanofabrication technology, MEMS and sensor technology, ultraprecision machining technology and equipment, and photoelectric testing technology and instrumentation.

**Ryutaro Maeda** joined the Mechanical Engineering Laboratory, Agency of Advanced Industrial Science and Technology (AIST) in Tsukuba in 1980 after earning his M.S. degree from the Graduate School of Tokyo University. He is the founder of UMEMSME (Research Centre of Ubiquitous MEMS and Micro Engineering) in AIST, was director there from 2010 to 2014, and served as the leader of several national projects, including the Green Sensor Network project and the JST CREST program. He has been a professor at Xi'an Jiaotong University since 2018. His current research interests include the application of wireless networked sensing for energy and safety management. He has published more than 300 papers in MEMS and related fields.